

Bifurcations of families of 1D-tori in 4D symplectic maps

Franziska Onken,^{1,2} Steffen Lange,^{1,2} Roland Ketzmerick,^{1,2} and Arnd Bäcker^{1,2}

¹⁾ *Technische Universität Dresden, Institut für Theoretische Physik and Center for Dynamics, 01062 Dresden, Germany*

²⁾ *Max-Planck-Institut für Physik komplexer Systeme, Nöthnitzer Straße 38, 01187 Dresden, Germany*

(Dated: 30 September 2018)

The regular structures of a generic 4D symplectic map with a mixed phase space are organized by one-parameter families of elliptic 1D-tori. Such families show prominent bends, gaps, and new branches. We explain these features in terms of bifurcations of the families when crossing a resonance. For these bifurcations no external parameter has to be varied. Instead, the longitudinal frequency, which varies along the family, plays the role of the bifurcation parameter. As an example we study two coupled standard maps by visualizing the elliptic and hyperbolic 1D-tori in a 3D phase-space slice, local 2D projections, and frequency space. The observed bifurcations are consistent with analytical predictions previously obtained for quasi-periodically forced oscillators. Moreover, the new families emerging from such a bifurcation form the skeleton of the corresponding resonance channel.

Bifurcations of invariant objects in dynamical systems lead to an abrupt qualitative change of the dynamics when an external parameter is varied smoothly. In higher-dimensional systems regular tori in phase space are organized around lower-dimensional tori. Thus, the bifurcations of these lower-dimensional tori have strong implications for the structures in phase space and the dynamics. In this work the case of 4D maps is considered for which families of 1D-tori organize the regular 2D-tori, see Fig. 1. It turns out, that these families undergo bifurcations without parameter variation. Hence, all stages of a bifurcation can be seen at once, which is visualized using 3D phase-space slices. At the same time this leads to a better understanding of the phase-space structure of resonance channels, which are of particular relevance for chaotic transport in higher-dimensional systems.

I. INTRODUCTION

The dynamics of higher-dimensional Hamiltonian systems is of interest to many fields from physics, mathematics, and chemistry. Such systems occur on scales ranging from atoms and molecules^{1–4}, over chemical reactions^{5–9} and particle accelerators^{10–12} to the solar system and galaxies^{13–17}. Moreover, they exhibit new transport phenomena like Arnold diffusion^{15,18–21}. Many of these examples are time-continuous systems, which can be reduced to discrete-time maps: For example, an autonomous Hamiltonian system with f degrees of freedom leads to a $2f$ -dimensional continuous system that can be reduced using energy conservation and a Poincaré section to a $(2f - 2)$ -dimensional symplectic map. Moreover, in some cases the dynamics is directly described by such maps^{22–24}. Thus, studying generic symplectic maps, which are numerically much more convenient, helps to

understand the dynamics of a wide range of systems.

Symplectic maps of dimension two are well understood, and generically possess a mixed phase space in which regular and chaotic motion coexist. The dynamics in the 2D phase space is organized by elliptic and hyperbolic periodic orbits. The local behavior around these points is described by the eigenvalues of the linearized dynamics. They contain either the frequency ν describing the regular motion on 1D-tori around an elliptic periodic orbit or the Lyapunov exponents of the stable and unstable

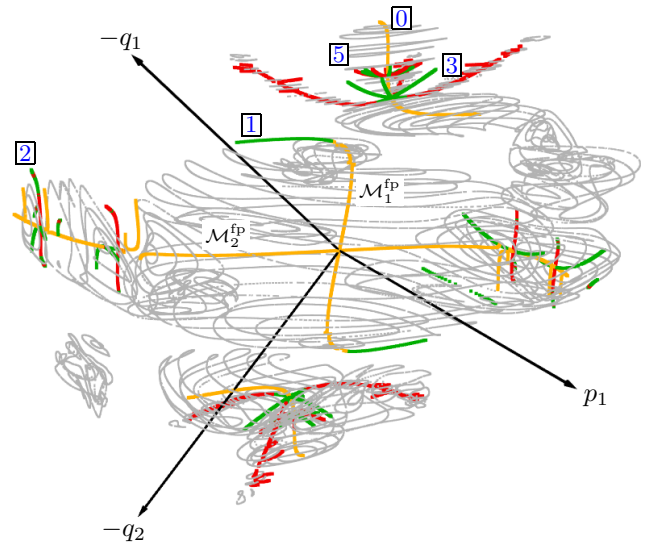


FIG. 1. The 4D phase space of two coupled standard maps Eq. (1), displayed in a 3D phase-space slice. Regular 2D-tori are shown as gray rings. The colored points forming lines are families of elliptic (orange, red) and hyperbolic (green) 1D-tori. The families $\mathcal{M}_1^{\text{fp}}$ and $\mathcal{M}_2^{\text{fp}}$ emanate from the EE fixed point \vec{u}_{fp} at the center $(p_1, q_1, q_2) = (0, 0.5, 0.5)$. Specific bifurcations are marked by blue boxed numbers and are discussed in detail in Sec. III. For a rotating view see <http://www.comp-phys.tu-dresden.de/supp/>.

directions of a hyperbolic periodic orbit. If a parameter of the map is varied, the frequency of an elliptic fixed point usually changes and crosses rational values, $\nu = n/m$. Depending on m different types of bifurcations occur, namely period-doubling ($|m| = 2$), touch-and-go ($|m| = 3, 4$), and m -tupling ($|m| \geq 4$) bifurcations^{25–29}.

The dynamics in maps of dimension four and higher has completely new features as invariant regular tori have an insufficient dimension to be barriers for the chaotic transport in phase space. This leads to new effects like Arnold diffusion^{15,18–21} along so-called resonance channels. In addition, the organization of the phase space of higher-dimensional maps is more complicated³⁰: In general, in a $2f$ -dimensional map elliptic n -dimensional tori^{31,32} are surrounded by (Cantor) families of elliptic $(n + 1)$ -dimensional tori^{33,34} with $n = 0, 1, \dots, f - 1$. Lower-dimensional tori can additionally originate from bifurcations of other lower-dimensional tori due to resonances^{35,36} or the break-up of resonant higher-dimensional tori³⁷. Moreover, such bifurcations give rise to families of hyperbolic lower-dimensional tori, also called whiskered tori^{18,38}, which are part of the so-called normally hyperbolic manifolds (NHMs). They play an important role for chaotic transport^{8,39}. Note that the families of lower-dimensional tori are rather Cantor families as they are interrupted by infinitely many gaps on finer and finer scales due to resonances and their corresponding bifurcations.

We focus on 4D symplectic maps in the generic regime far from integrability which occur in many practical applications^{1,4,23,40}. In contrast, many former studies cover near-integrable systems, in which normal form tools^{32,36,37} can be used. In order to visualize such a generic 4D phase space, we employ 3D phase-space slices⁴¹, i.e. for every point of an orbit the three remaining coordinates inside the slice are considered in a 3D plot, see Fig. 1 for an example and Sec. II for a brief introduction. In a 4D map the regular motion takes place on 2D-tori, some of which are shown as gray rings in Fig. 1. In addition, there are 1D-tori, also called invariant circles or fixed lines, which can be either elliptic or hyperbolic^{33,38,42}. In the 3D phase-space slice they correspond to single points, which occur in one-parameter families and thus lead to continuous looking lines. Such families of elliptic 1D-tori are either attached to elliptic-elliptic fixed points or arise from bifurcations, see orange and red lines in Fig. 1, respectively. These families are the skeleton of the regular motion as each 1D-torus is surrounded by 2D-tori and the families of 1D-tori form a hierarchy³⁰ analogously to the island-around-island hierarchy in 2D maps. The hyperbolic 1D-tori occur in families as well, see green lines in Fig. 1. Furthermore, there are 0D periodic orbits, which can have stabilities elliptic-elliptic (EE), elliptic-hyperbolic (EH), hyperbolic-hyperbolic (HH), and complex-unstable (CU). They can also undergo bifurcations under parameter variation^{43–46}, which, however, is not the subject of this study.

The aim of this paper is to explain the characteristics of

the families of elliptic 1D-tori in detail, namely their gaps, bends, and branches as visible in Fig. 1. It turns out that these structures can be understood as bifurcations of the families caused by crossing resonances. While bifurcations usually arise under parameter variation, we observe all stages of a bifurcation in a single phase space without varying any parameter. This is possible because the longitudinal, or intrinsic, frequency of the 1D-tori varies smoothly along the family and plays the role of the bifurcation parameter. We observe that local 2D projections of the bifurcations in 3D phase-space slices remarkably resemble phase-space plots of bifurcations of periodic orbits in 2D maps. This is consistent with normal form results for quasi-periodically forced oscillators³⁶ and investigations in 3D volume-preserving maps⁴⁷. Moreover, the families of 1D-tori arising from a bifurcation due to a crossing resonance are also the skeleton of this resonance channel.

This paper is organized as follows: In Sec. II we introduce as generic example system two coupled standard maps and give a short review of its dynamics. In Sec. III bifurcations of families of 1D-tori are categorized and illustrated in detail. This local behavior is complemented by an investigation of global properties in Sec. IV. Finally, Sec. V gives a summary and an outlook. The special case of symmetry breaking bifurcations is described in Appendix A and a short review of the used algorithm to compute elliptic and hyperbolic 1D-tori is given in Appendix B.

II. DYNAMICS IN 4D MAPS

We consider as a generic example two coupled standard maps⁴⁸, $(p_1, p_2, q_1, q_2) \mapsto (p'_1, p'_2, q'_1, q'_2)$,

$$\begin{aligned} p'_1 &= p_1 + \frac{K_1}{2\pi} \sin(2\pi q'_1) + \frac{\xi_{12}}{2\pi} \sin(2\pi(q'_1 + q'_2)) \\ p'_2 &= p_2 + \frac{K_2}{2\pi} \sin(2\pi q'_2) + \frac{\xi_{12}}{2\pi} \sin(2\pi(q'_1 + q'_2)) \\ q'_1 &= q_1 + p_1 \\ q'_2 &= q_2 + p_2, \end{aligned} \quad (1)$$

where $p_{1,2} \in [-0.5, 0.5]$ and $q_{1,2} \in [0, 1)$ and periodic boundary conditions are imposed in each coordinate. The resulting map is symplectic. The parameters K_1 and K_2 control the nonlinearity of the individual 2D standard maps in (p_1, q_1) and (p_2, q_2) , respectively. The parameter ξ_{12} introduces a coupling between the two degrees of freedom. We choose $K_1 = 2.25$, $K_2 = 3.0$ and $\xi_{12} = 1.0$, such that the system is strongly coupled and far from integrability⁴¹. The fixed point $\vec{u}_{\text{fp}} = (p_1, p_2, q_1, q_2) = (0, 0, 0.5, 0.5)$ is of type EE. The eigenvalues $(\lambda_1^{\text{fp}}, \bar{\lambda}_1^{\text{fp}}, \lambda_2^{\text{fp}}, \bar{\lambda}_2^{\text{fp}})$ of the linearized dynamics around \vec{u}_{fp} are $(\exp(\pm i 2\pi \nu_1^{\text{fp}}), \exp(\pm i 2\pi \nu_2^{\text{fp}}))$ with $(\nu_1^{\text{fp}}, \nu_2^{\text{fp}}) = (0.30632, 0.12173)$. The mapping Eq. (1) has been the subject of several studies^{19,43,46,49,50}.

An orbit started at some initial point in the 4D phase space leads to a sequence of points (p_1, p_2, q_1, q_2) under the map Eq. (1). To visualize such an orbit we use a 3D phase-space slice⁴¹, defined by thickening a 3D hyperplane Γ in the 4D phase space. Explicitly, we consider the slice defined by

$$\Gamma_\varepsilon = \left\{ (p_1, p_2, q_1, q_2) \mid |p_2 - p_2^*| \leq \varepsilon \right\} \quad (2)$$

with $p_2^* = 0$ and $\varepsilon = 10^{-4}$ as it provides a good view of most structures of the map Eq. (1). Whenever a point of an orbit lies within Γ_ε , the remaining coordinates (p_1, q_1, q_2) are displayed in a 3D plot, see Fig. 1. Objects of the 4D phase space typically appear in the 3D phase-space slice with a dimension reduced by one like sketched in Fig. 2, provided the object intersects with the slice. Thus, a typical 2D-torus (gray) leads to two or more 1D lines (black). A typical 1D-torus (blue line) leads to two or more points (orange spheres). As 1D-tori occur in families, they lead to lines in the 3D phase-space slice, e.g. the orange families in Fig. 1. A periodic orbit will in general not be visible, unless at least one of its points lies in the 3D phase-space slice.

In order to relate bifurcations to resonances, phase space objects are represented in frequency space. Using frequency analysis^{14,51} we associate with each 2D-torus its two fundamental frequencies $(\nu_1, \nu_2) \in [0, 1]^2$, see Fig. 2. These are displayed in the frequency space, see Fig. 3, where the gray points represent 2D-tori obtained by starting 10^8 initial conditions with randomly chosen $p_1, p_2 \in [-0.2, 0.2]$, $q_1, q_2 \in [0.3, 0.7]$ in the 4D phase space. Each frequency pair is calculated from $N = 4096$ iterations using a Fourier method (Sec. 4.2.4 in Ref.⁵¹). Note that there are no rotational tori in the system at the chosen parameters. To decide whether an orbit is regular we use the frequency criterion $\max(|\nu_1 - \tilde{\nu}_1|, |\nu_2 - \tilde{\nu}_2|) < 10^{-7}$, where the second frequency pair $(\tilde{\nu}_1, \tilde{\nu}_2)$ is calculated from N further iterations. This leads to nearly $3 \cdot 10^6$ regular 2D-tori. The frequencies (ν_1, ν_2) are only defined up to a unimodular transformation^{52,53}. Start-

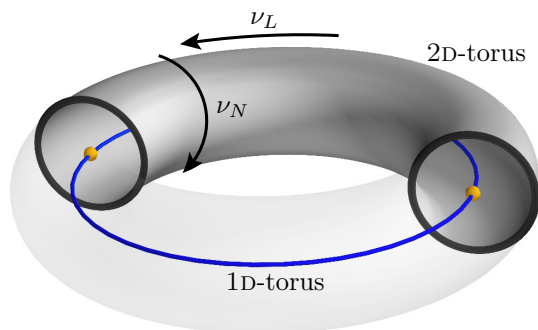


FIG. 2. Sketch of structures in the 3D phase-space slice. A 2D-torus (gray) appears generically as two rings (black) while a 1D-torus (blue line) leads to two points (orange spheres). The longitudinal and the normal direction with corresponding frequencies ν_L and ν_N are indicated by arrows.

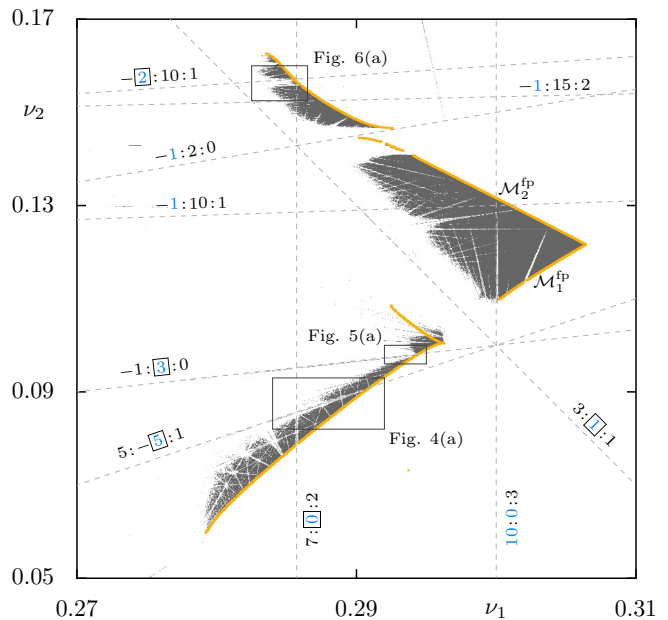


FIG. 3. Frequency space of regular 2D-tori (gray points) of the coupled standard maps, Eq. (1). The rightmost tip $(\nu_1^{\text{fp}}, \nu_2^{\text{fp}}) = (0.30632, 0.12173)$ corresponds to the EE fixed point \vec{u}_{fp} . From there the two main families of elliptic 1D-tori $\mathcal{M}_1^{\text{fp}}$ and $\mathcal{M}_2^{\text{fp}}$ (orange) emanate. Some resonances are shown as dashed lines with labels $m_1 : m_2 : n$. In every label the factor $|m_N|$ is marked in blue. The boxed values correspond to the bifurcations labeled in Fig. 1. The three black boxes indicate magnifications shown in Fig. 4(a), Fig. 5(a) and Fig. 6(a).

ing from the EE fixed point with frequencies $(\nu_1^{\text{fp}}, \nu_2^{\text{fp}})$ we have used the 3D phase-space slice to obtain a consistent representation in frequency space by applying appropriate unimodular transformations such that neighboring regions in phase space are mapped to neighboring regions in frequency space⁴¹.

The frequency space is covered by resonance lines $m_1 : m_2 : n$, on which the frequencies fulfill

$$m_1 \cdot \nu_1 + m_2 \cdot \nu_2 = n \quad (3)$$

where m_1, m_2, n are integers without common divisor. Some resonance lines that are relevant in the following are displayed in Fig. 3 as dashed lines.

On a 1D-torus the dynamics is described by only one longitudinal frequency ν_L which is also called intrinsic or internal frequency or rotation number. If the 1D-torus is elliptic, it is surrounded by 2D-tori. For a sequence of such 2D-tori converging to a 1D-torus, one of the two frequencies (ν_1, ν_2) converges towards the longitudinal frequency ν_L , see Fig. 2. The limit of the other frequency corresponds to the normal frequency ν_N describing the rotation of points normal to the elliptic 1D-torus³³. Therefore, the families of 1D-tori are represented by the edges in frequency space, see Fig. 3. The normal frequency ν_N may also be obtained from the linearized motion around the 1D-torus⁵⁴.

There are two families $\mathcal{M}_1^{\text{fp}}$, $\mathcal{M}_2^{\text{fp}}$ of elliptic 1D-tori emanating from the EE fixed point \bar{u}_{fp} , shown as orange lines in Fig. 3. On the family $\mathcal{M}_1^{\text{fp}}$ the frequency ν_1 corresponds to the longitudinal frequency ν_L and ν_2 to the normal one ν_N , i.e. a resonance $m_1 : m_2 : n$ crossing $\mathcal{M}_1^{\text{fp}}$ corresponds to $m_L : m_N : n$. On $\mathcal{M}_2^{\text{fp}}$ it is the other way around, i.e. $m_1 : m_2 : n$ corresponds to $m_N : m_L : n$. As discussed in the following section, m_N is the decisive parameter for the categorization of bifurcations of families of 1D-tori. The respective values of m_N are marked as blue numbers in Fig. 3.

III. BIFURCATIONS OF FAMILIES OF 1D-TORI

In this section we explain the structures that occur along the main families $\mathcal{M}_1^{\text{fp}}$ and $\mathcal{M}_2^{\text{fp}}$ in Fig. 1, i.e. new emerging branches, gaps, and strong bends, by bifurcations. These bifurcations occur as the frequencies ν_L and ν_N , which vary smoothly along every family, cross resonance lines, see Fig. 3. To study the structures at a bifurcation we compute the newly emerging elliptic and hyperbolic families of 1D-tori, see Appendix B for details, and relate all involved objects in phase space and in frequency space.

Bifurcations of 1D-tori were also investigated for quasi-periodically forced oscillators³⁶ and 3D volume-preserving maps⁴⁷, and it was found that the normal coefficient m_N of the crossing resonance is the relevant parameter to categorize such bifurcations. In the following, we discuss the different cases of m_N to explain the structures in phase space starting with the generic case $|m_N| \geq 4$ (branches) and then continue with $|m_N| = 3$ (branches), $|m_N| = 2$ (gaps), $|m_N| = 1$ (bends) and $|m_N| = 0$ (gaps). The resonances used as examples are marked by dashed lines in Fig. 3 with labels in which the values of m_N are blue and boxed. Further examples have been investigated⁵⁵. There also exist symmetry breaking bifurcations, which are discussed in Appendix A.

This categorization of bifurcations is analogous to 2D maps, where the resonance condition reads $m \cdot \nu = n$ and m is the relevant number to categorize the bifurcations^{25–27,29}. It turns out that for $m_N = m$ the features of the bifurcations of families of 1D-tori in 4D maps resemble bifurcations of fixed points in 2D maps.

In the following we refer to the family of 1D-tori which is crossed by a resonance as *main family*. Families of elliptic 1D-tori created in a bifurcation also undergo bifurcations which leads to a whole hierarchy³⁰. All bifurcations occur independent of the hierarchy and of the origin of the family, i.e. whether they arise from fixed points or from other bifurcations. Thus, without loss of generality we concentrate on the first level of the hierarchy, i.e. in the following the main family is always either $\mathcal{M}_1^{\text{fp}}$ or $\mathcal{M}_2^{\text{fp}}$ indicated in orange.

In the visualizations we observe that the gaps within the families of 1D-tori created in a bifurcation get very small close to the main family. It is known that for elliptic

families of 1D-tori attached at EE fixed points these gaps get exponentially small with the distance to the fixed point^{33,50}. Thus, we conjecture that also the gaps in the families of 1D-tori arising from a bifurcation get exponentially small close to the main family.

To visualize and analyze the bifurcations, we use in addition to the frequency space and the 3D phase-space slice also local 2D projections of the 3D phase-space slice. They are useful to relate the results to both 2D bifurcations and normal form results. The basic methods and concepts are introduced in detail in the following section.

A. Branches: $|m_N| \geq 4$

For $|m_N| \geq 4$ one obtains generic bifurcations of a family of 1D-tori in which one elliptic and one hyperbolic family of 1D-tori are created. As the geometry of the 1D-tori is dictated^{30,37,47} by the crossing resonance condition $m_L : m_N : n$, each 1D-torus consists of $\text{gcd}(m_L, m_N)$ disjoint but dynamically connected loops. Furthermore, the families of 1D-tori appear in a typical 3D phase-space slice as alternating $|m_N|$ elliptic and $|m_N|$ hyperbolic branches.

As an example we discuss in detail the $5 : -5 : 1$ resonance intersecting $\mathcal{M}_1^{\text{fp}}$, i.e. $|m_N| = 5$, see Fig. 3. This resonance causes the red and green branches in phase space marked by $\boxed{5}$ in Fig. 1.

This example is visualized in several ways in Fig. 4: Figure 4(a) shows a zoom of the frequency space of Fig. 3 close to the crossing point of the resonance and the main family $\mathcal{M}_1^{\text{fp}}$. In Fig. 4(b) the structure is shown in a 3D phase-space slice, which is a rotated magnification of Fig. 1. There one can see five hyperbolic (green) and five elliptic (red) branches emerging out of the main family $\mathcal{M}_1^{\text{fp}}$ (orange). Note that the branches consist of individual points, where each point corresponds to an intersection of a 1D-torus with the 3D phase-space slice. Every 1D-torus of these branches consists of $\text{gcd}(5, -5) = 5$ disjoint loops.

For a clear visualization of the stages of the bifurcation, we consider in Figs. 4(c)–(e) *local 2D projections* from the 3D phase-space slice of Fig. 4(b) onto 2D planes. They show several orbits started in the respective plane, such that the 2D-tori are represented as gray rings and the 1D-tori as colored points. Note that the chosen 2D projections help to focus on a specific part of the 3D phase-space slice. The normal vector of the planes for the shown 2D projections is chosen along the family $\mathcal{M}_1^{\text{fp}}$ of 1D-tori (orange). The positions of the local 2D projections are indicated in Fig. 4(a) by the frequencies of the elliptic 1D-tori involved in Figs. 4(c)–(e), marked with encircled characters \textcircled{c} to \textcircled{e} , and in Fig. 4(b) by enlarged points. By this variation of the position of the local 2D projection along $\mathcal{M}_1^{\text{fp}}$ the different stages of the bifurcation become visible without varying any parameter of the map.

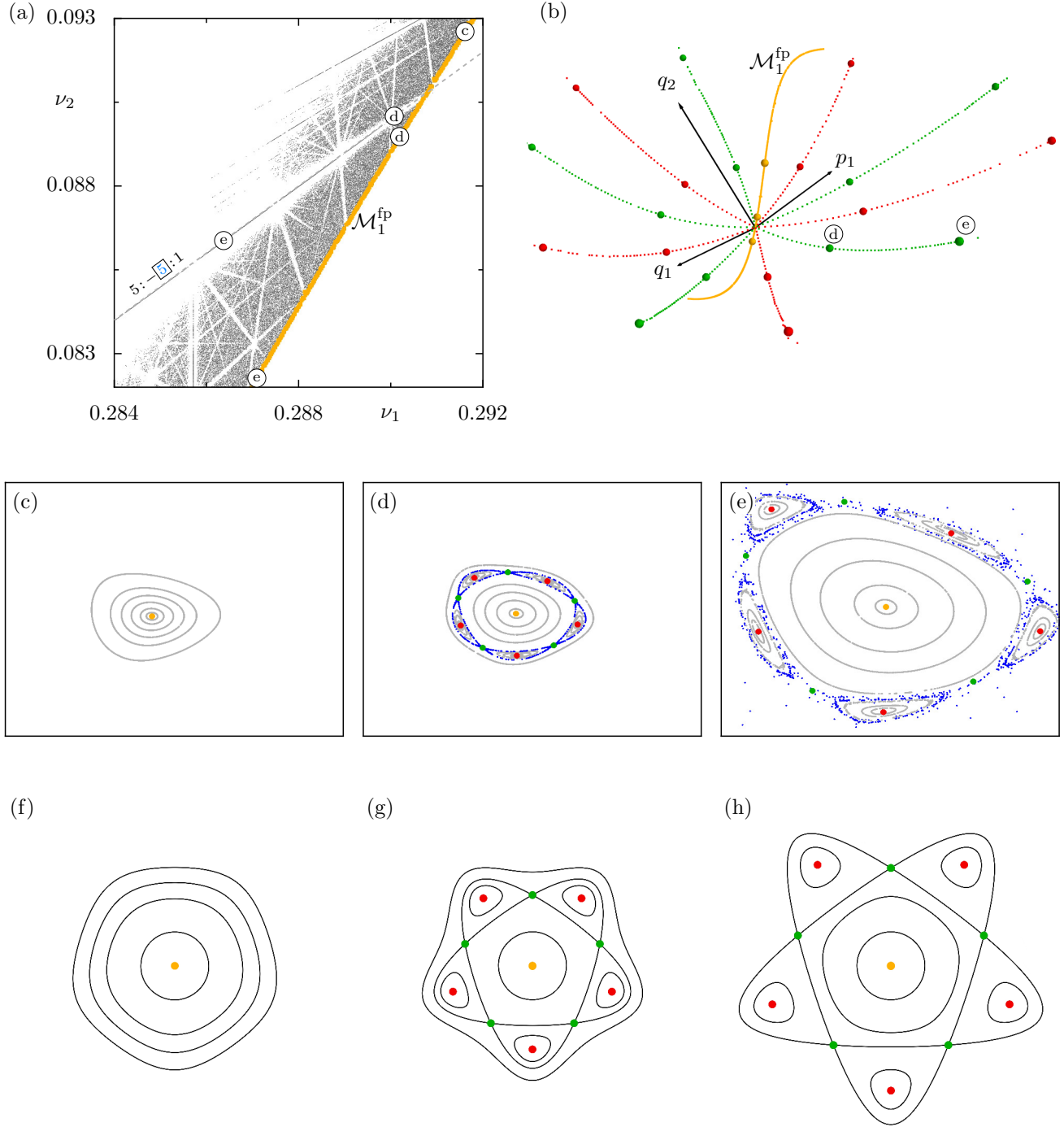


FIG. 4. Visualization of the $5 : -5 : 1$ resonance intersecting $\mathcal{M}_1^{\text{fp}}$. (a) Zoom of frequency space, Fig. 3, with resonance line (dashed gray line), regular 2D-tori (gray) and a part of $\mathcal{M}_1^{\text{fp}}$ (orange). (b) Magnified and rotated view of the structure labeled with $\mathcal{M}_1^{\text{fp}}$ in the 3D phase-space slice in Fig. 1 with elliptic (red) and hyperbolic 1D-tori (green). The orange line is a part of $\mathcal{M}_1^{\text{fp}}$. (c)–(e) Sequence of local 2D projections from the 3D phase-space slice onto a plane with normal vector $\vec{n} = (-0.338, -0.644, 0.687)$ illustrating the stages of the bifurcation with regular 2D-tori (gray rings), elliptic 1D-tori (red, orange), and hyperbolic 1D-tori (green). The 1D-tori appearing in the local 2D projections (colored points) are marked by encircled letters © to © in (a) and by larger spheres in (b). (f)–(h) Contour plots of the simplified normal form³⁶ $f(I, \phi; \lambda, \mu) = \lambda I - I^2 + \mu^{m-3} A (2I)^{m/2} \cos(m\phi)$ with parameters $m = 5$, $\mu^{m-3} \cdot A \cdot 2^{m/2} = -0.4$ (f) before, $\lambda = -0.2$, (g) right after, $\lambda = 0.2$, and (h) further away from the bifurcation, $\lambda = 0.4$. The colored points mark the equilibria. For a rotating view of (b) see <http://www.comp-phys.tu-dresden.de/supp/>.

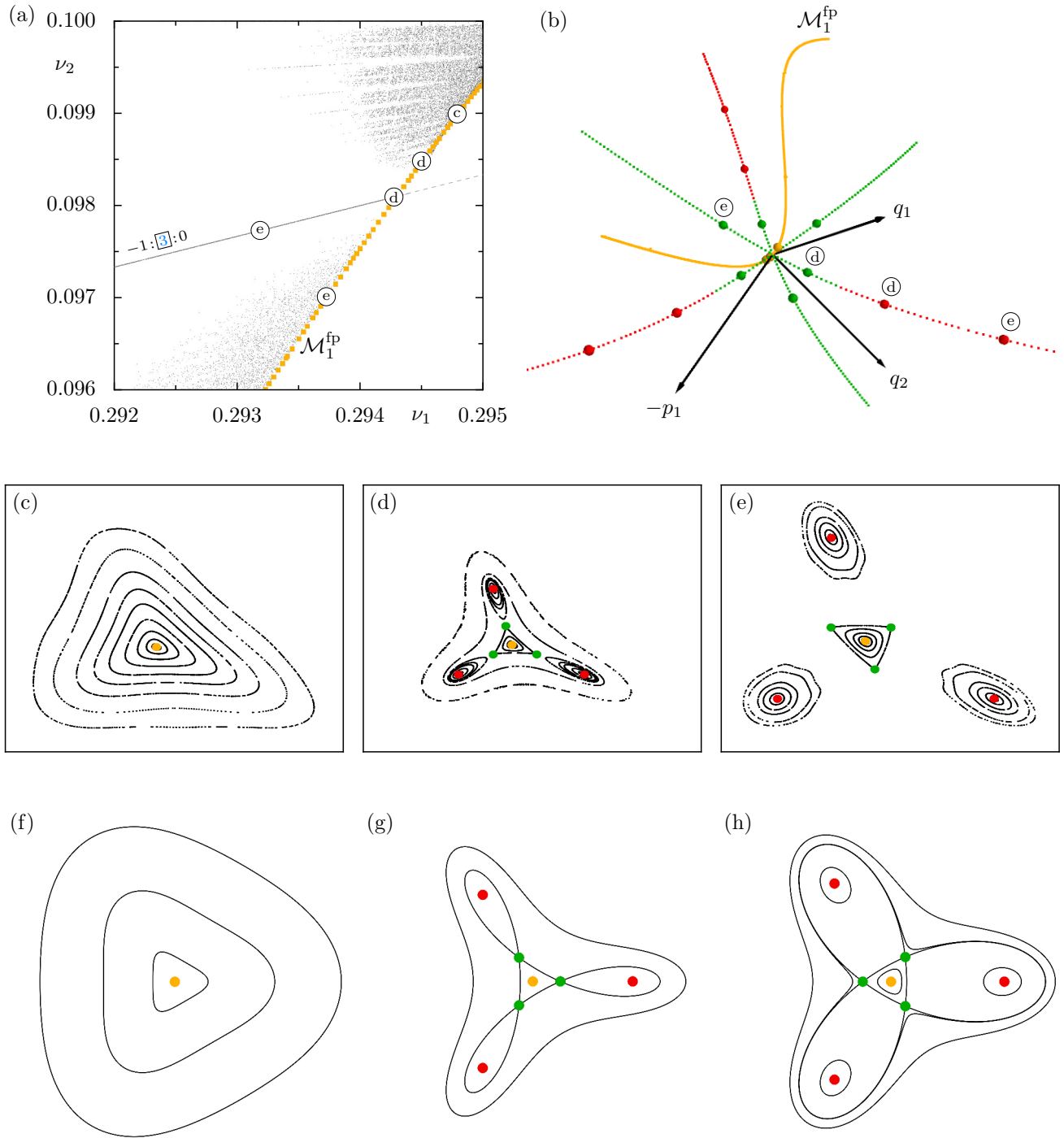


FIG. 5. Visualization of the $-1 : 3 : 0$ resonance similar to Fig. 4. (c)–(e) Local 2D projections with normal vector $\vec{n} = (-0.336, -0.672, 0.66)$. (f)–(h) Contour plots of the normal form³⁶ $f(p, q; \lambda, A) = \lambda \frac{p^2+q^2}{2} - \left(\frac{p^2+q^2}{2}\right)^2 + A(q^3 - 3p^2q)$, $A = 0.05$, (f) before, $\lambda = -0.016$, (g) after the saddle-node part, $\lambda = -0.004$, and (h) after the touch-and-go bifurcation, $\lambda = 0.01$. For a rotating view of (b) see <http://www.comp-phys.tu-dresden.de/supp/>.

The resulting 2D plots look remarkably similar to a period-5-tupling bifurcation in 2D maps. However, the interpretation is different: an isolated point in the local 2D projections corresponds to a 1D-torus while a closed line corresponds to a 2D-torus. For a 2D map these objects would correspond to a periodic point and a regular torus, respectively.

These observations are consistent with normal form results obtained for parametrized families of quasi-periodically forced Hamiltonian oscillators³⁶. Figures 4(f)–(h) show contour plots of the corresponding normal form for different stages of the bifurcation. The stable and unstable equilibrium points are marked in red and green, respectively. Figures 4(f)–(h) demonstrate how an “island chain” consisting of five stable and five unstable equilibria emerges out of the 1D-torus in the center. After the bifurcation the distance of the islands to the center increases. The same behavior is observed in Figs. 4(c)–(e) along the main family. This resemblance supports the conjecture³⁶ that the normal form results obtained for quasi-periodically forced oscillators also apply to generic fully coupled systems. Note that the normal form does not describe any gaps in the arising families, which are visible in Fig. 4(b).

It is worth emphasizing that the new elliptic and hyperbolic families of 1D-tori shown in Fig. 4(b) and their surrounding form the resonance channel in phase space. In frequency space in Fig. 4(a) this whole phase-space region collapses to the resonance line $5 : -5 : 1$.

In Fig. 4(d) and Fig. 4(e) chaotic orbits with initial conditions inside the resonance channel are included as blue points. In Fig. 4(d) the chaotic orbits in the resonance channel are effectively confined by KAM tori, such that they cannot escape the channel on short time scales. In contrast the chaotic orbits in Fig. 4(e) clearly escape from the channel. These two regimes can also be seen in frequency space, Fig. 4(a). Near the bifurcation (upper Ⓓ), i.e. close to the orange main family, the channel is embedded in gray 2D-tori, but further away (upper Ⓒ), such confining 2D-tori cease to exist.

B. Branches: $|m_N| = 3$

Bifurcations with $|m_N| = 3$ are more complicated: Initially, an elliptic and a hyperbolic family of 1D-tori emerge in a saddle-node bifurcation. The hyperbolic family collapses at the main family and reemerges from it. Thus, this region is considerably deprived of regular tori. The families appear in a 3D phase-space slice as three hyperbolic and three elliptic branches.

As an example we consider the $-1 : 3 : 0$ resonance intersecting $\mathcal{M}_1^{\text{fp}}$. In Fig. 5 a series of plots analogous to Fig. 4 is shown. The $-1 : 3 : 0$ resonance leads to elliptic (red) and hyperbolic (green) branches in phase space, marked by [3] in Fig. 1, and a large open resonance channel in frequency space, see Fig. 5(a). Especially, in the 3D phase-space slice in Fig. 5(b) one recognizes that

the elliptic branches (red) do not start at the main family $\mathcal{M}_1^{\text{fp}}$ (orange) but at the saddle-node bifurcation, i.e. the point where the hyperbolic (green) and the elliptic (red) part of the branch meet.

The stages of this bifurcation can again be understood by means of the local 2D projections. In Figs. 5(c)–(e) projections of orbits started in the respective 2D plane are shown. The positions of the local 2D projections are indicated in Fig. 5(a) by circled characters and in Fig. 5(b) by larger spheres. These pictures not only resemble all stages of a 2D touch-and-go period tripling bifurcation, but also match qualitatively with normal form predictions³⁶, which are shown in Figs. 5(f)–(h). Note that this normal form of the period-tripling already includes the saddle-node bifurcation in contrast to the corresponding one for 2D area-preserving maps^{25,26}, for which, despite of this, the period-tripling is still commonly observed to be preceded by the saddle-node bifurcation^{28,56,57}.

In both series (c)–(e) and (f)–(h) the first figure shows the phase space before the bifurcation with just deformed 2D-tori. The second one shows the stage after the saddle-node bifurcation including the three new hyperbolic families of 1D-tori (green) and the three islands each centered around a family of elliptic 1D-tori (red). The last stage is the “touch-and-go” part, where the three hyperbolic branches (green) meet at the main family $\mathcal{M}_1^{\text{fp}}$ and cross each other. The third figures show the phase space after this stage, i.e. where all branches just continue to spread out from the main family $\mathcal{M}_1^{\text{fp}}$.

C. Gaps: $|m_N| = 2$

Bifurcations with $|m_N| = 2$ cause gaps in the main family of elliptic 1D-tori in the sense that the family contains a segment of hyperbolic 1D-tori: Firstly, the main family of elliptic 1D-tori changes its stability to hyperbolic while one elliptic family emerges, appearing as two branches in the 3D phase-space slice. Secondly, the main family of now hyperbolic 1D-tori becomes elliptic again and a hyperbolic family emerges, also appearing as two branches in the 3D phase-space slice. This bifurcation is similar to a combination of a direct and an inverse period-doubling bifurcation in 2D maps.

As an example we consider the $-2 : 10 : 1$ resonance, marked by [2] in Figs. 1 and 3, which intersects $\mathcal{M}_2^{\text{fp}}$. Figure 6(a) is a zoom of the frequency space in Fig. 3 and shows a bend of the main family (orange), which appears to “converge” to the resonance line from either side. Figure 6(b) shows the structure in the 3D phase-space slice. The main family $\mathcal{M}_2^{\text{fp}}$ (orange) is interrupted by a hyperbolic part (green, marked by α) and when turning hyperbolic a family of elliptic 1D-tori (red) emerges. When the main family turns elliptic again, a family of hyperbolic 1D-tori (green, marked by β) arises.

For this bifurcation we have not been able to find a sequence of local 2D projections which clearly shows

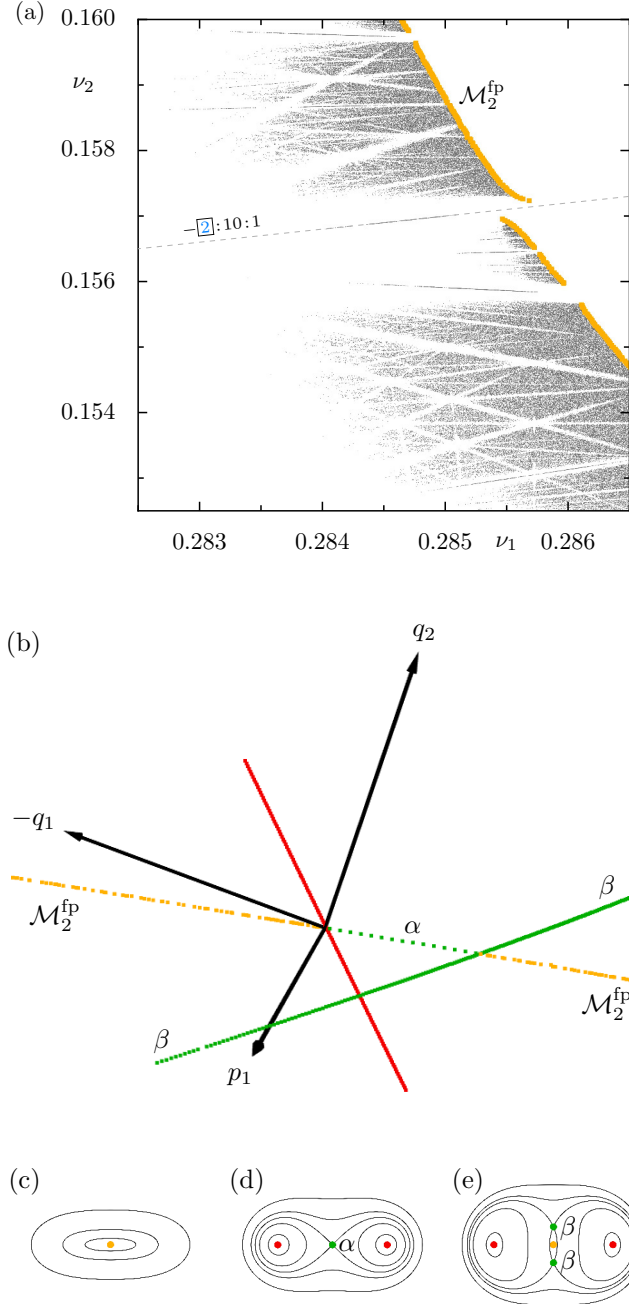


FIG. 6. Visualization of the $-2:10:1$ resonance as in Fig. 4. (b) The orange family $\mathcal{M}_2^{\text{fp}}$ temporarily changes stability to hyperbolic (α) due to the $|m_N| = 2$ bifurcation. At each end of the hyperbolic part (α) new elliptic (red) and hyperbolic (green, β) families emerge. (c)–(e) Contour plots of the normal form³⁶ $f(p, q; \delta, A) = (\delta+a)\frac{p^2+q^2}{2} - \left(\frac{p^2+q^2}{2}\right)^2 + A(q^2-p^2)$, $A = 0.05$, $a = 0.1$, (c) before, $\delta = -0.21$, (d) after the first period-doubling, $\delta = -0.1$, and (e) after the second period-doubling bifurcation, $\delta = 0.02$. For a rotating view of (b) see <http://www.comp-phys.tu-dresden.de/supp/>.

the different stages. Thus, we now use the intuition gained from bifurcations with $|m_N| \geq 3$ (sections III A and III B) to understand the connection between the 3D phase-space slice in Fig. 6(b) and normal form plots³⁶ in Figs. 6(c)–(e). In these figures the stages of the bifurcation are shown from left to right: (c) shows the phase space before the bifurcations, (d) after the first (direct) period doubling and (e) after the second (inverse) period doubling bifurcation. In (e) the emerging hyperbolic branches (green) lie on a line perpendicular to the line of the new elliptic branches (red). This geometric relation is also recognizable in the 3D phase-space slice, see rotating view of Fig. 6(b).

D. Bends: $|m_N| = 1$

Bifurcations with $|m_N| = 1$ cause prominent bends in a family of elliptic 1D-tori on either side of the crossing resonance, which leads to pronounced gaps. While the

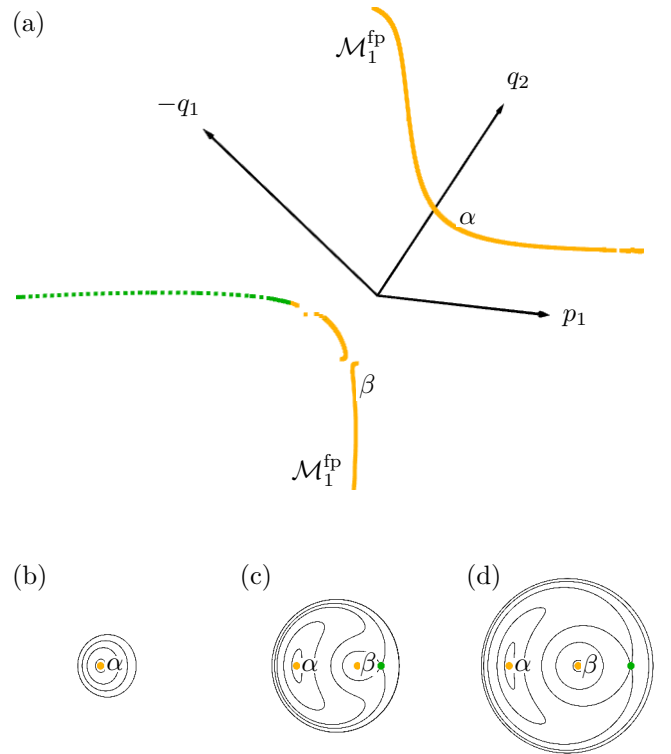


FIG. 7. Visualization of the $3:1:1$ resonance as in Fig. 4. (a) The orange family labeled with α is a part of $\mathcal{M}_1^{\text{fp}}$ and bends away due to the $|m_N| = 1$ bifurcation. (b)–(d) Contour plots of the normal form³⁶ $f(p, q; \delta, A) = \delta\frac{p^2+q^2}{2} - \left(\frac{p^2+q^2}{2}\right)^2 + Aq$, $A = -0.006$, (b) before, $\delta = -0.04$, (c) right after, $\delta = 0.08$, and (d) later after, $\delta = 0.16$, the bifurcation. (d) shows how the elliptic branch β takes over the role of the branch α . For a rotating view of (a) see <http://www.comp-phys.tu-dresden.de/supp/>.

elliptic branch on one side of the gap just bends, the one on the other side gets hyperbolic at some point. The point where this family changes its stability is similar to a 2D saddle-node bifurcation. In the 4D case this “new” elliptic family continues the family of 1D-tori that stays elliptic beyond the gap. The $|m_N| = 1$ bifurcations lead to bends in frequency space, which has also been observed for 3D volume-preserving maps⁴⁷.

As an example the $3 : 1 : 1$ resonance intersecting $\mathcal{M}_1^{\text{fp}}$ is considered, because it causes a prominent bend in phase space and in frequency space, marked by [1](#) in Figures 1 and 3. Note that also all the smaller bends of $\mathcal{M}_1^{\text{fp}}$ and $\mathcal{M}_2^{\text{fp}}$ visible in Fig. 1 are caused by crossing resonances with $|m_N| = 1$.

Figure 7(a) shows the family $\mathcal{M}_1^{\text{fp}}$ (orange) at the bend with the hyperbolic branch (green) in a 3D phase-space slice. Coming from the top of Fig. 7(a) the upper elliptic branch α (orange) stays elliptic and bends to the right. Below that another elliptic branch β and a hyperbolic branch emerge from a saddle-node bifurcation. In particular, the elliptic branch β continues the elliptic branch α beyond the gap. This observation is consistent with the normal form results³⁶ shown in Figs. 7(b)–(d). The stable equilibrium in Fig. 7(b) corresponds to the upper branch labeled with α in Fig. 7(a). The plot (c) shows the normal form just after the saddle-node bifurcation which creates the hyperbolic and the lower elliptic branch β . The last plot (d) visualizes how the elliptic branch β moves to the center and takes over the role of the original elliptic family α .

E. $m_N = 0$

The condition $m_N = 0$ means that the longitudinal frequency ν_L of a family of 1D-tori crosses a rational value n/m_L . This leads to the break-up of the resonant elliptic 1D-torus into a chain of periodic orbits of alternating EE and EH stability. This looks like the well-known 2D Poincaré-Birkhoff scenario⁵⁸ embedded in a 2D manifold composed of a family of elliptic 1D-tori.

We consider the $7 : 0 : 2$ resonance as example, marked by [0](#) in Figures 1 and 3. This case was already discussed in detail³⁰ as limiting case of an uncoupled rank-1-resonance. The resulting chain of EE and EH periodic orbits and a close-by 1D-torus are shown in a color projection⁵⁹ onto the 3D phase-space slice in Fig. 8. For orientation, the orange points of the main family $\mathcal{M}_1^{\text{fp}}$ from Fig. 1 are included.

Note that this is the only type of resonance which also affects families of hyperbolic 1D-tori as they just have a longitudinal frequency ν_L . Hence, this is the only way to get deeper into a hyperbolic hierarchy: If the longitudinal frequency crosses a rational value, the resonant hyperbolic 1D-torus breaks up in a chain of alternating HH and EH periodic points. The EH periodic points have again a family of hyperbolic 1D-tori attached³³. Like in the elliptic case the dynamics restricted to the manifold

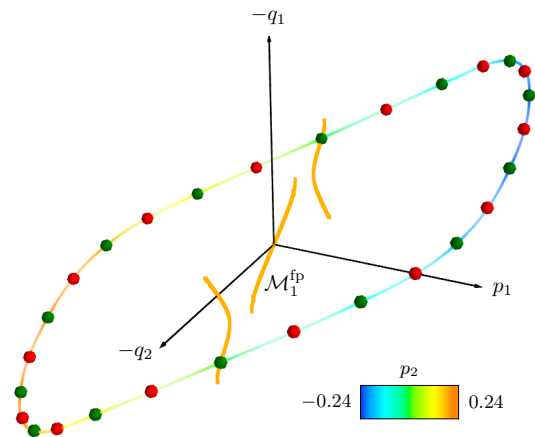


FIG. 8. Chain of periodic orbits of type EE (red) and EH (green), which are the remnants of a 1D-torus of $\mathcal{M}_1^{\text{fp}}$ that fulfilled the $7 : \text{0} : 2$ resonance. In addition the points in the 3D phase-space slice of the family $\mathcal{M}_1^{\text{fp}}$ and a 3D projection of a close-by 1D-torus with the fourth coordinate encoded as color is shown for comparison. For a rotating view see <http://www.comp-phys.tu-dresden.de/supp/>.

composed of a family of hyperbolic 1D-tori looks similar to a 2D Poincaré-Birkhoff scenario.

IV. GLOBAL BEHAVIOR

In the previous section the local structure of bifurcations of families of 1D-tori has been considered. Now we want to discuss the global behavior, i.e. the geometry and the properties of the newly created 1D-tori far away from the bifurcation. Furthermore, we discuss the geometry of a family of 1D-tori whose corresponding resonance line intersects both main families $\mathcal{M}_1^{\text{fp}}$ and $\mathcal{M}_2^{\text{fp}}$.

A. Properties of bifurcated families of 1D-tori

Near the bifurcation, i.e. near the crossing of a resonance line and a main family, the underlying geometry is described by the corresponding normal form. On the other hand, further away from the bifurcation, pairs of elliptic and hyperbolic 1D-tori can be thought of as remnants of broken resonant 2D-tori, which has been shown³⁷ using normal form analysis for resonances of order ≥ 5 and illustrated for a generic 4D map³⁰. Note that this is analogous to the well-known Poincaré-Birkhoff scenario in 2D maps. The break-up of a resonant 2D-torus suggests that the remnant elliptic and hyperbolic 1D-tori have similar longitudinal frequency ν_L and a similar action $I = \oint_{\gamma} \sum_{i=1,2} p_i dq_i$ with γ being a path along the remnant 1D-torus. Moreover, both 1D-tori resemble the geometry of the original 2D-torus,

As an illustration we consider the $-1 : 15 : 2$ resonance, see Fig. 3, for which an action-frequency plot is

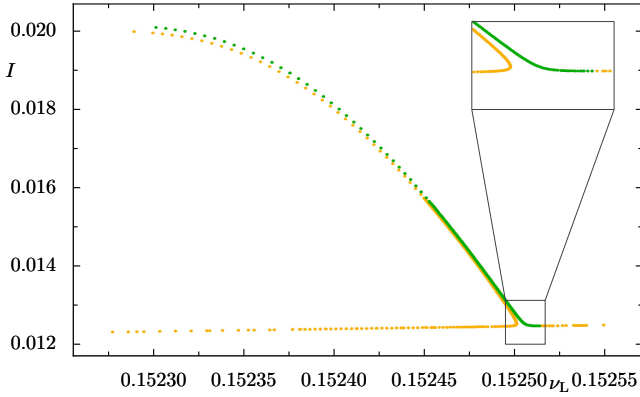


FIG. 9. Action-frequency plot for the $-1 : 15 : 2$ resonance crossing the main family $\mathcal{M}_2^{\text{fp}}$. The elliptic 1D-tori are shown in orange and the hyperbolic ones in green.

shown in Fig. 9. The bifurcation with $|m_N| = 1$ takes place at $\nu_L \approx 0.152506$ and a pair of an elliptic and a hyperbolic family of 1D-tori branches off the main family $\mathcal{M}_2^{\text{fp}}$ with increasing action. Their two actions $I(\nu_L)$ match remarkably well far away from the bifurcation. An even better agreement was observed⁵⁵ for generic bifurcations, i.e. $|m_N| \geq 5$.

In addition, we also find a relation in the normal behavior. For bifurcations with $|m_N| \geq 5$ we observe for a pair of 1D-tori with equal values of ν_L that 2π times the normal frequency ν_N of the elliptic 1D-torus and the Lyapunov-exponent λ_N of the hyperbolic one match surprisingly well even far away from the bifurcation. The relation of ν_N and λ_N close to the bifurcation can be explained using the normal form expression for the $|m_N| \geq 5$ bifurcation. From the linearized dynamics, see e.g. Eq. (5.4.19) in Ref.²⁹, it follows that $2\pi\nu_N = \lambda_N$. In addition, we also observe for $|m_N| = 1$ bifurcations a very good match of λ_N and $2\pi\nu_N$ away from the bifurcation.

As discussed in the previous section, the families of 1D-tori bifurcating from the main family when crossing a resonance are the skeleton of the corresponding resonance channel. Our findings suggest that one can estimate the properties of a hyperbolic 1D-torus within such a resonance channel from its elliptic counterpart, which is numerically much easier to compute. This is especially interesting as the Lyapunov-exponents are relevant for the chaotic transport within the channel.

B. Connection of bifurcations

An interesting global connection happens if a resonance crosses both main families $\mathcal{M}_1^{\text{fp}}$ and $\mathcal{M}_2^{\text{fp}}$. While the local behavior at each crossing point is described by the normal form of the corresponding bifurcation, the geometry of such connections is non-trivial. For example, consider the $m_1 : m_2 : n = 10 : 0 : 3$ resonance

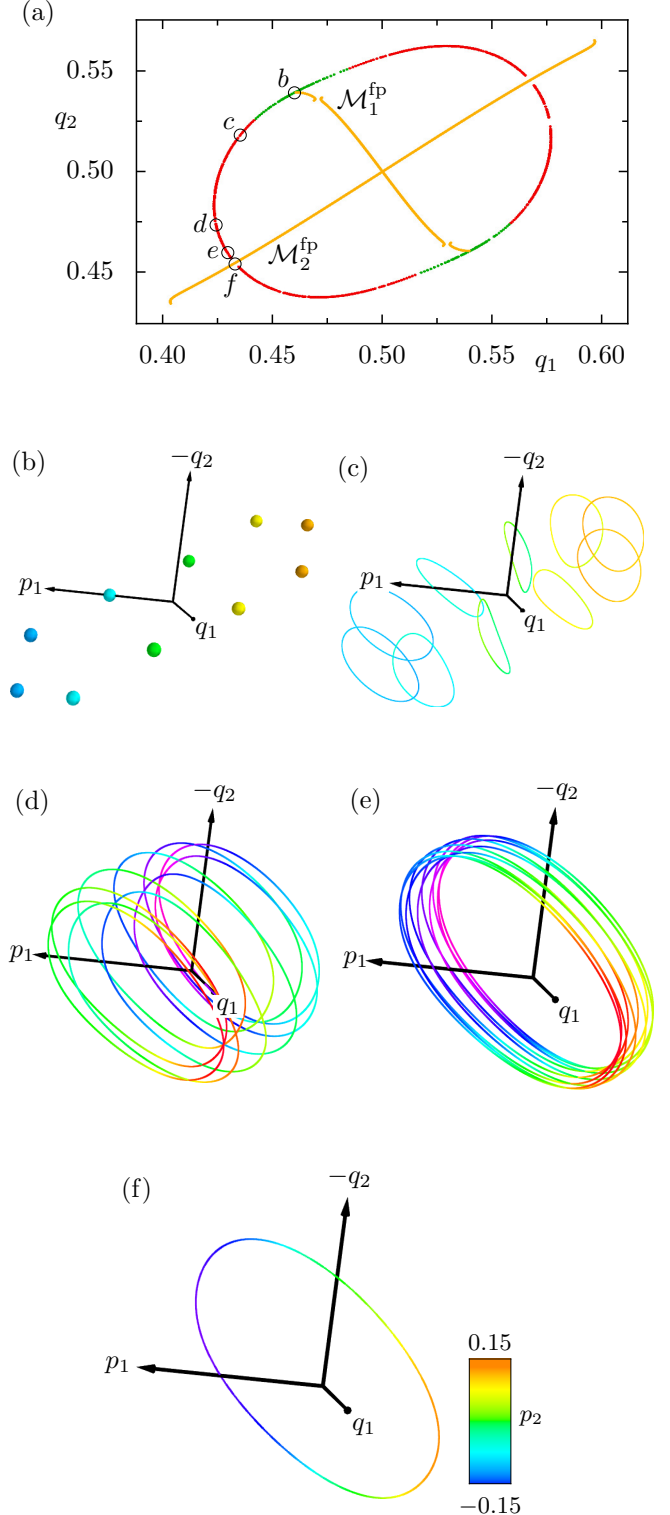


FIG. 10. Visualization of $10 : 0 : 3$ resonance connecting both main families. (a) The main families $\mathcal{M}_1^{\text{fp}}$, $\mathcal{M}_2^{\text{fp}}$ (orange) and one of the two connecting families of 1D-tori (elliptic – red, hyperbolic – green) are shown. The series (b)–(f) shows the 3D projections of 1D-tori at the positions marked in (a) with the p_2 -coordinate encoded as color. For a rotating view see <http://www.comp-phys.tu-dresden.de/supp/>.

in Fig. 3 for which m_N is given by $m_2 = 0$ at the intersection with $\mathcal{M}_1^{\text{fp}}$ while at the intersection with $\mathcal{M}_2^{\text{fp}}$ it is given by $m_1 = 10$. Hence, the coefficients m_1, m_2 exchange their roles along the family of 1D-tori. This implies, that the longitudinal and the normal radius, see Fig. 2, of the original, resonant 2D-tori interchange along the resonance, i.e. the normal radius increases and the longitudinal radius decreases.

We now illustrate the geometry of this connection by a visualization in phase space. For this we use the 3D phase-space slice, which in case of the considered $10 : 0 : 3$ resonance can be reduced further to a plot in the $(q_1 - q_2)$ -plane. This is possible as the p_1 coordinate is zero for all points lying in the 3D phase-space slice due to symmetry, see Appendix A. Figure 10(a) shows one of the two families of 1D-tori (green and red points) of the $10 : 0 : 3$ resonance connecting the main families $\mathcal{M}_1^{\text{fp}}$ and $\mathcal{M}_2^{\text{fp}}$ (orange).

The change in geometry of the 1D-tori when going from $\mathcal{M}_1^{\text{fp}}$ to $\mathcal{M}_2^{\text{fp}}$ along the resonance is illustrated in Fig. 10(b)–(f) by color projections, i.e. the fourth coordinate p_2 is encoded in color. When the resonance crosses $\mathcal{M}_1^{\text{fp}}$ it causes a $|m_N| = 0$ bifurcation, i.e. the 1D-torus with $\nu_L = 3/10$ breaks up in a chain of EE and EH periodic points as described in Sec. III E, see Fig. 10(b). At the EE periodic points two elliptic families of 1D-tori and at the EH periodic points one hyperbolic family of 1D-tori are attached. One of the two elliptic families is embedded in $\mathcal{M}_1^{\text{fp}}$, see Fig. 4c in Ref.³⁰, while the other elliptic family of 1D-tori is, as in Sec. IV A, the counterpart to the hyperbolic family of 1D-tori. Following the hyperbolic family away from the bifurcation the geometry of the broken 2D-torus becomes visible. For instance, the 1D-torus shown in Fig. 10(c) consists of ten disjoint rings, which are arranged like an orbit on a 2D-torus with resonant longitudinal frequency $\nu_L = 3/10$.

With increasing distance from the family $\mathcal{M}_1^{\text{fp}}$ the rings get larger and start to overlap in the 3D projection, see Fig. 10(d). This continues until the ten rings are oriented in the longitudinal direction like an orbit on a 2D-torus with resonant normal frequency $\nu_N = 3/10$, see Fig. 10(e). Finally, all rings collapse onto one 1D-torus of $\mathcal{M}_2^{\text{fp}}$, see Fig. 10(f). This corresponds to a type $|m_N| = 10$ bifurcation caused by the $10 : 0 : 3$ resonance crossing $\mathcal{M}_2^{\text{fp}}$. Thus, the connection between $\mathcal{M}_1^{\text{fp}}$ and $\mathcal{M}_2^{\text{fp}}$ along the resonance can be seen as exchange of the longitudinal and the normal radius of the original 2D-tori.

Note that we observe a surprising change of stability along the connection shown in Fig. 10(a). The connecting family starts hyperbolic (green) at the EH periodic orbit (b) and later changes stability to elliptic (red). At the same point the corresponding elliptic family of 1D-tori turns hyperbolic. Thus one could call this a transcritical bifurcation of a 1D-torus because an exchange of stability occurs along the family. Whether this is a generic phenomenon for such connections or specific to the investigated resonance and system requires further

investigation.

V. SUMMARY AND OUTLOOK

In this paper we investigate the bifurcations of families of elliptic 1D-tori which occur when they cross resonances. We observe all stages of the bifurcations in the phase space of one 4D map without varying any parameter. This is possible because the longitudinal and normal frequencies of the families vary smoothly along a family. As regular 2D-tori are arranged around the skeleton of families of elliptic 1D-tori their bifurcations leading to gaps, bends, and new branches crucially determine the organization of the regular structures in phase space. To visualize the structures we use the frequency space, 3D phase-space slices, and local 2D projections of the 3D phase-space slices.

On a resonance the longitudinal and the normal frequency fulfill a condition $m_L \cdot \nu_L + m_N \cdot \nu_N = n$. The crucial number determining the type of the bifurcation is m_N . If a family of elliptic 1D-tori crosses a resonance with $|m_N| = 1$, it will form prominent bends. A $|m_N| = 2$ bifurcation leads to an intermediate change of stability and hence to a gap in the regular structures. At each end of the gap a new family emerges. The most complicated structure is caused by $|m_N| = 3$ bifurcations. Before the bifurcation a pair of families of elliptic and hyperbolic 1D-tori is created from which the hyperbolic family collapses onto the main family and re-emerges afterwards with opposite orientation. For generic bifurcations with $|m_N| \geq 4$ one elliptic and one hyperbolic family of 1D-tori emerges directly from the main family. In the 3D phase-space slice the new families appear as $2 \cdot m_N$ branches of alternating stability. Using local 2D projections we demonstrate that all the results are consistent with normal form predictions and numerically support the conjecture that they are also valid for generic 4D maps³⁶. In terms of these 2D projections the bifurcations in 4D maps resemble bifurcations of fixed points in 2D maps.

The families of 1D-tori emerging from a bifurcation form the skeleton of the corresponding resonance channel. We investigate the families along a resonance channel even far away from the bifurcation. For bifurcations with $|m_N| \geq 4$ we find an interesting relation between the new elliptic and hyperbolic families: for each pair of elliptic and hyperbolic 1D-tori the normal frequency ν_N and the Lyapunov exponent λ_N match surprisingly well, $2\pi\nu_N \approx \lambda_N$. Thus, based on the elliptic family it is possible to gain information on the hyperbolic family, which is numerically much harder to find and to compute. Moreover, for resonances intersecting the two main families of 1D-tori an interesting, non-trivial geometric connection is observed.

There are also several interesting open questions and future applications: Where and why do families of elliptic and hyperbolic 1D-tori end? How do bifurcations of periodic points connect with the picture obtained from the

bifurcations of families of 1D-tori? Furthermore, based on the skeleton of a resonance channel one can investigate how the stable and unstable manifolds of the families of hyperbolic 1D-tori govern the chaotic transport. Moreover, understanding the geometry of junctions of resonance channels is of importance as they play an important role for chaotic transport in the Arnold web.

ACKNOWLEDGEMENTS

We are grateful for discussions with Henk Broer, Holger Dullin, Àlex Haro, Àngel Jorba, Srihari Keshavamurthy, Alejandro Luque, and Jim Meiss. Furthermore, we acknowledge support by the Deutsche Forschungsgemeinschaft under grant KE 537/6-1.

All 3D visualizations were created using MAYAVI⁶⁰.

Appendix A: Symmetry breaking bifurcations

For bifurcations of periodic orbits in 2D area-preserving maps it is well-known that the presence of symmetries leads to additional types of bifurcations^{28,61,62}. In this section we demonstrate that symmetries also cause new types of bifurcations of families of 1D-tori in addition to the ones described in Sec. III. Moreover, we discuss further implications of the presence of symmetries for families of 1D-tori.

The symmetries of a variant of the reversible⁶³ 4D map Eq. (1), were already studied⁴⁶. From this one obtains the reversing symmetry operator

$$\begin{aligned} S_1 : \quad p' &= p \\ q' &= -q - p \end{aligned} \quad (\text{A1})$$

with $p = (p_1, p_2)$, $q = (q_1, q_2)$, for the map Eq. (1). A reversing symmetry⁶⁴ is an involution, $S_1^2 = \text{Id}$, and allows for a simple expression of the inverse map, $f^{-1} = S_1 \circ f \circ S_1$. Using an inversion, i.e. changing the sign of all coordinates, one obtains a further reversing symmetry⁶⁵

$$\begin{aligned} S_2 : \quad p' &= -p \\ q' &= q + p \end{aligned} \quad (\text{A2})$$

As an example we explain the unusual bifurcations corresponding to the resonances $-1 : 2 : 0$ and $-1 : 10 : 1$ shown in Fig. 3 by these two symmetries.

For the $-1 : 2 : 0$ resonance intersecting $\mathcal{M}_2^{\text{fp}}$ with $|m_N| = 1$ one would expect, according to Sec. III D, a strong bend of the family in phase space. Instead, in phase space a large gap with new branches at each end and in frequency space prominent bends are observed. Thus, this corresponds to the geometry found for the case $|m_N| = 2$, see Sec. III C. However, for the $-1 : 2 : 0$ resonance the new branches are not dynamically connected, i.e. twice the number of families arise. The symmetry operator S_1 provides the mapping between these two families. This demonstrates the

symmetry-breaking nature of this bifurcation, similar to the symmetry-breaking period-doubling of periodic orbits in area-preserving maps. Note that for $|m_N| = 1$ we only observe symmetry breaking when m_L is even.

For the $-1 : 10 : 1$ resonance intersecting $\mathcal{M}_2^{\text{fp}}$ one would also expect the $|m_N| = 1$ behavior. Instead, the geometry in phase space even looks like a $|m_N| = 4$ bifurcation, i.e. in a 3D phase-space slice four elliptic branches emerge directly from the main family. Again these branches are not dynamically connected: one pair of them is related by S_1 , while the other pair is related by S_2 . Hence, this is a double symmetry breaking bifurcation of a family of 1D-tori. Note that the corresponding four families of hyperbolic 1D-tori were not found due to technical difficulties.

The presence of symmetries has further implications for families of 1D-tori: Consider a 1D-torus with longitudinal frequency ω , which can be represented by $x(\theta)$ with $f^{\pm 1}(x(\theta)) = x(\theta \pm \omega)$ and $\theta \in [0, 2\pi)$, see Eq. (B2). Such a 1D-torus is mapped by a symmetry S to a 1D-torus with same frequency, as from $f^{\pm 1} = S \circ f^{\mp 1} \circ S$ and $S^2 = \text{Id}$ follows $(f^{\mp 1} \circ S)(x(\theta)) = S(x(\theta \pm \omega))$. For instance, each of the families $\mathcal{M}_1^{\text{fp}}$ and $\mathcal{M}_2^{\text{fp}}$ is mapped by a symmetry to a family of 1D-tori. As the families $\mathcal{M}_1^{\text{fp}}$ and $\mathcal{M}_2^{\text{fp}}$ are the only families which contain the EE fixed point \vec{u}_{fp} , which is invariant under the symmetries S_1 and S_2 , there are only two options: either $S_i(\mathcal{M}_1^{\text{fp}}) = \mathcal{M}_1^{\text{fp}}$ and $S_i(\mathcal{M}_2^{\text{fp}}) = \mathcal{M}_2^{\text{fp}}$, or $S_i(\mathcal{M}_1^{\text{fp}}) = \mathcal{M}_2^{\text{fp}}$ and $S_i(\mathcal{M}_2^{\text{fp}}) = \mathcal{M}_1^{\text{fp}}$. As the range of frequencies ω of these families $\mathcal{M}_1^{\text{fp}}$ and $\mathcal{M}_2^{\text{fp}}$ does not coincide, see Fig. 3, the first option holds, i.e. the families $\mathcal{M}_1^{\text{fp}}$ and $\mathcal{M}_2^{\text{fp}}$ are invariant under S_1 and S_2 . Furthermore, we observe that every 1D-torus of these families has exactly two intersection points x_1, x_2 with the 3D slice $p_2 = 0$. The points $S_1(x_1)$, $S_1(x_2)$, $S_2(x_1)$, $S_2(x_2)$ also have $p_2 = 0$, since $|p|$ is conserved under S_1 and S_2 , see Eqs. (A1) and (A2). Thus, this set of points has to coincide with the set of points $\{x_1, x_2\}$. This is only possible if the intersection points are of the form $x_1 = (0, 0, q_1, q_2)$, $x_2 = (0, 0, -q_1, -q_2)$. For this reason the families $\mathcal{M}_1^{\text{fp}}$ and $\mathcal{M}_2^{\text{fp}}$ intersect with the 2D plane defined by $p_1 = p_2 = 0$ on a line rather than just in a point. To show this for other families of 1D-tori similar arguments may be applied.

Appendix B: Computation of 1D-tori

To compute invariant 1D-tori we use a Fourier expansion method^{50,66}. In the following we will give a brief review⁵⁵ to comment on specific choices of parameters used in this paper. The basic idea of the method is to describe a 1D-torus by a finite Fourier series

$$x(\theta) = a_0 + \sum_{k=1}^N a_k \cos(k\theta) + \sum_{k=1}^N b_k \sin(k\theta) \quad (\text{B1})$$

with 4-dimensional coefficients a_k, b_k and an angle $\theta \in [0, 2\pi)$. For highly deformed 1D-tori we used up to $N = 240$ coefficients.

On every invariant 1D curve with longitudinal frequency $\omega = 2\pi\nu_L$ one has

$$f(x(\theta)) = x(\theta + \omega), \quad (\text{B2})$$

where f denotes the map Eq. (1). Thus one can define an error of the approximation by

$$F_N(x(\theta_i)) = f(x(\theta_i)) - x(\theta_i + \omega) \quad (\text{B3})$$

which is evaluated on the grid $\theta_i = 2\pi i/(2N + 1)$, $i \in \{0, 1, \dots, 2N\}$. For a fixed ω a high-dimensional Newton search in the coefficients a_k and b_k is used to find zeros of $F_N(x(\theta))$. We stop the search if an error of $\|F_N(x(\hat{\theta}))\|_\infty < 10^{-12}$ is reached where $\hat{\theta}$ denotes a 10 times finer grid than θ . Note that the invariant curve described by $x(\theta)$ is the same object as $x(\theta + \varphi)$ for any $\varphi \in \mathbb{R}$. To get rid of this freedom, one needs to add a uniqueness condition. As we want to visualize the 1D-tori in a 3D phase-space slice with $p_2^* = 0$, we use $p_2 = 0$ as this condition.

For the Newton search an initial guess for the coefficients a_k, b_k and the longitudinal frequency ω is needed. If at least one 1D-torus of a family of 1D-tori is known, an initial guess for a close-by 1D-torus of this family can be obtained by extrapolating within the $(4(2N + 1) + 1)$ -dimensional space spanned by a_k, b_k and ω . As continuation parameter the Euclidian distance in this space is used⁶⁶. Then, the whole family can be computed using a predictor-corrector continuation. Thus, the crucial task is to either find an initial 1D-torus of the family and compute its Fourier coefficients or to obtain a guess for the Fourier coefficients from geometric considerations. This is described in the following by three approaches:

(i) The first approach is to start from 2D-tori and apply the geometric contraction method³⁰ to obtain elliptic 1D-tori. This is particularly useful as it allows for obtaining 1D-tori beyond bends and large gaps where a direct continuation method usually fails.

(ii) For families attached at EE or EH periodic points \vec{u} one can use each pair of elliptic eigenvalues $\exp(\pm i 2\pi\nu)$ and the corresponding eigenvectors $\vec{\xi}, \vec{\bar{\xi}}$ of the linearized map at the periodic point to define an initial guess, i.e. $a_0 = \vec{u}$, $a_1 = 2\varepsilon\Re(\vec{\xi})$, $b_1 = 2\varepsilon\Im(\vec{\xi})$, $\omega = 2\pi\nu + \Delta\omega$ with small $|\varepsilon|$ and $|\Delta\omega|$.

(iii) The previous two approaches do not work for families of hyperbolic 1D-tori arising from bifurcations. For bifurcations with odd $|m_N|$ these families are computed by extrapolating the elliptic branches through the main family, see Fig. 4(b). For even $|m_N|$ we use the following approach⁵⁵: From Sec. IV A it is known that the longitudinal frequencies of the new elliptic and hyperbolic families match. Thus, we can choose a rational value n/m in their frequency range and find the corresponding EH or HH m -periodic orbit which is embedded in the

hyperbolic family according to Sec. III E. As these periodic orbits roughly lie on a 1D-torus, we approximate a nearby 1D-torus by an ellipse using the mean of the periodic points \vec{C} and two of the periodic points \vec{A} and \vec{B} , i.e. $a_0 = \vec{C}$, $a_1 = \vec{A} - \vec{C} + \vec{\delta}_a$, $b_1 = \vec{B} - \vec{C} + \vec{\delta}_b$, $\omega = n/m + \Delta\omega$ with small $\|\vec{\delta}_b\|$, $\|\vec{\delta}_a\|$, and $|\Delta\omega|$.

- ¹S. Gekle, J. Main, T. Bartsch, and T. Uzer, “Extracting multidimensional phase space topology from periodic orbits”, *Phys. Rev. Lett.* **97**, 104101 (2006).
- ²P. Schlagheck and A. Buchleitner, “Stable classical configurations in strongly driven helium”, *Physica D* **131**, 110–124 (1999).
- ³S. Keshavamurthy, “Dynamical tunneling in molecules: quantum routes to energy flow”, *Int. Rev. Phys. Chem.* **26**, 521–584 (2007).
- ⁴R. Paškauskas, C. Chandre, and T. Uzer, “Dynamical bottlenecks to intramolecular energy flow”, *Phys. Rev. Lett.* **100**, 083001 (2008).
- ⁵T. Uzer, C. Jaffé, J. Palacián, P. Yanguas, and S. Wiggins, “The geometry of reaction dynamics”, *Nonlinearity* **15**, 957–992 (2002).
- ⁶M. Toda, T. Komatsuzaki, T. Konishi, R. S. Berry, and S. A. Rice (editors) *Geometric Structures of Phase Space in Multidimensional Chaos: Applications to Chemical Reaction Dynamics in Complex Systems*, volume 130 of *Advances in Chemical Physics*, John Wiley & Sons, Inc., Hoboken, New Jersey (2005).
- ⁷A. Shojiguchi, C.-B. Li, T. Komatsuzaki, and M. Toda, “Fractional behavior in multidimensional Hamiltonian systems describing reactions”, *Phys. Rev. E* **76**, 056205 (2007), erratum *ibid.* **77**, 019902 (2008).
- ⁸H. Waalkens, R. Schubert, and S. Wiggins, “Wigner’s dynamical transition state theory in phase space: classical and quantum”, *Nonlinearity* **21**, R1–R118 (2008).
- ⁹P. Manikandan and S. Keshavamurthy, “Dynamical traps lead to the slowing down of intramolecular vibrational energy flow”, *Proc. Natl. Acad. Sci. USA* **111**, 14354–14359 (2014).
- ¹⁰A. Bazzani, S. Siboni, and G. Turchetti, “Action diffusion for symplectic maps with a noisy linear frequency”, *J. Phys. A* **30**, 27–36 (1997).
- ¹¹M. N. Vrahatis, H. Isliker, and T. C. Bountis, “Structure and breakdown of invariant tori in a 4-D mapping model of accelerator dynamics”, *Int. J. Bifurcat. Chaos* **7**, 2707–2722 (1997).
- ¹²Y. Papaphilippou, “Detecting chaos in particle accelerators through the frequency map analysis method”, *Chaos* **24**, 024412 (2014).
- ¹³S. Udry and D. Pfenniger, “Stochasticity in elliptical galaxies”, *Astron. & Astrophys.* **198**, 135–149 (1988).
- ¹⁴J. Laskar, “The chaotic motion of the solar system: A numerical estimate of the size of the chaotic zones”, *Icarus* **88**, 266–291 (1990).
- ¹⁵P. M. Cincotta, “Arnold diffusion: an overview through dynamical astronomy”, *New Astron. Rev.* **46**, 13–39 (2002).
- ¹⁶R. I. Páez and C. Eftymiopoulos, “Trojan resonant dynamics, stability, and chaotic diffusion, for parameters relevant to exoplanetary systems”, *Celest. Mech. Dyn. Astr.* **121**, 139–170 (2015).
- ¹⁷C. Jung and E. E. Zotos, “Order and chaos in a three dimensional galaxy model”, *Mechanics Research Communications* **69**, 45–53 (2015).
- ¹⁸V. I. Arnol’d, “Instability of dynamical systems with several degrees of freedom”, *Sov. Math. Dokl.* **5**, 581–585 (1964).
- ¹⁹K. Kaneko and R. J. Bagley, “Arnold diffusion, ergodicity, and intermittency in coupled standard mapping”, *Phys. Lett. A* **110**, 435–440 (1985).
- ²⁰P. Lochack, “Arnold diffusion; A compendium of remarks and questions”, in C. Simó (editor) “Hamiltonian Systems with Three or More Degrees of Freedom”, volume 533 of *NATO ASI Series: C - Mathematical and Physical Sciences*, 168–183, Kluwer Academic Publishers, Dordrecht (1999).
- ²¹A. Malyshev and L. Chizhova, “Arnold diffusion in a system

- with 2.5 degrees of freedom: Classical and quantum mechanical approaches”, *J. Exp. Theor. Phys.* **110**, 837–844 (2010).
- ²²P. Gaspard and S. A. Rice, “Hamiltonian mapping models of molecular fragmentation”, *J. Phys. Chem.* **93**, 6947–6957 (1989).
- ²³R. E. Gillilan and G. S. Ezra, “Transport and turnstiles in multidimensional Hamiltonian mappings for unimolecular fragmentation: Application to van der Waals predissociation”, *J. Chem. Phys.* **94**, 2648–2668 (1991).
- ²⁴H. S. Dumas and J. Laskar, “Global dynamics and long-time stability in Hamiltonian systems via numerical frequency analysis”, *Phys. Rev. Lett.* **70**, 2975–2979 (1993).
- ²⁵K. R. Meyer, “Generic bifurcation of periodic points”, *Trans. Amer. Math. Soc.* **149**, 95–107 (1970).
- ²⁶A. D. Brjuno, “Instability in a Hamiltonian system and the distribution of asteroids”, *Math. USSR Sbornik* **12**, 271–312 (1970).
- ²⁷A. M. Ozorio de Almeida, *Hamiltonian Systems: Chaos and Quantization*, Cambridge University Press, Cambridge (1988).
- ²⁸J.-M. Mao and J. B. Delos, “Hamiltonian bifurcation theory of closed orbits in the diamagnetic Kepler problem”, *Phys. Rev. A* **45**, 1746–1761 (1992).
- ²⁹P. Leboeuf and A. Mouchet, “Normal forms and complex periodic orbits in semiclassical expansions of Hamiltonian systems”, *Ann. Phys. (N.Y.)* **275**, 54–112 (1999).
- ³⁰S. Lange, M. Richter, F. Onken, A. Bäcker, and R. Ketzmerick, “Global structure of regular tori in a generic 4D symplectic map”, *Chaos* **24**, 024409 (2014).
- ³¹L. H. Eliasson, “Perturbations of stable invariant tori for Hamiltonian systems”, *Ann. Sc. Norm. Super. Pisa, Cl. Sci.* **15**, 115–147 (1988).
- ³²J. Pöschel, “On elliptic lower dimensional tori in Hamiltonian systems”, *Math. Z.* **202**, 559–608 (1989).
- ³³À. Jorba and J. Villanueva, “On the normal behaviour of partially elliptic lower-dimensional tori of Hamiltonian systems”, *Nonlinearity* **10**, 783–822 (1997).
- ³⁴À. Jorba and J. Villanueva, “The fine geometry of the Cantor families of invariant tori in Hamiltonian systems”, in C. Casacuberta, R. Miró-Roig, J. Verdera, and S. Xambó-Descamps (editors) “European Congress of Mathematics”, volume 202 of *Progress in Mathematics*, 557–564, Birkhäuser Basel (2001).
- ³⁵M. Gemmi and E. Toderico, “Stability and geometry of third-order resonances in four-dimensional symplectic mappings”, *Celest. Mech. Dyn. Astr.* **67**, 181–204 (1997).
- ³⁶H. Broer, H. Hanßmann, À. Jorba, J. Villanueva, and F. Wagener, “Normal-internal resonances in quasi-periodically forced oscillators: a conservative approach”, *Nonlinearity* **16**, 1751–1791 (2003).
- ³⁷E. Toderico, “Analysis of resonant structures of four-dimensional symplectic mappings, using normal forms”, *Phys. Rev. E* **50**, R4298–R4301 (1994).
- ³⁸E. Zehnder, “Generalized implicit function theorems with applications to some small divisor problems, II”, *Comm. Pure Appl. Math.* **29**, 49–111 (1976).
- ³⁹S. Wiggins, “On the geometry of transport in phase space I. Transport in k -degree-of-freedom Hamiltonian systems, $2 \leq k < \infty$ ”, *Physica D* **44**, 471–501 (1990).
- ⁴⁰A. Luque and J. Villanueva, “A KAM theorem without action-angle variables for elliptic lower dimensional tori”, *Nonlinearity* **24**, 1033–1080 (2011).
- ⁴¹M. Richter, S. Lange, A. Bäcker, and R. Ketzmerick, “Visualization and comparison of classical structures and quantum states of four-dimensional maps”, *Phys. Rev. E* **89**, 022902 (2014).
- ⁴²S. M. Graff, “On the conservation of hyperbolic invariant tori for Hamiltonian systems”, *J. Diff. Eqs.* **15**, 1–69 (1974).
- ⁴³D. Pfenniger, “Numerical study of complex instability. I. Mappings”, *Astron. & Astrophys.* **150**, 97–111 (1985).
- ⁴⁴J. E. Howard and R. S. MacKay, “Linear stability of symplectic maps”, *J. Math. Phys.* **28**, 1036–1051 (1987).
- ⁴⁵G. Contopoulos and A. Giorgilli, “Bifurcations and complex instability in a 4-dimensional symplectic mapping”, *Meccanica* **23**, 19–28 (1988).
- ⁴⁶H. Kook and J. D. Meiss, “Periodic orbits for reversible, symplectic mappings”, *Physica D* **35**, 65–86 (1989).
- ⁴⁷H. R. Dullin and J. D. Meiss, “Quadratic volume-preserving maps: Invariant circles and bifurcations”, *SIAM J. Appl. Dyn. Syst.* **8**, 76–128 (2009).
- ⁴⁸C. Froeschlé, “Numerical study of a four-dimensional mapping”, *Astron. & Astrophys.* **16**, 172–189 (1972).
- ⁴⁹J. Laskar, “Frequency analysis for multi-dimensional systems. global dynamics and diffusion”, *Physica D* **67**, 257–281 (1993).
- ⁵⁰À. Jorba and M. Ollé, “Invariant curves near Hamiltonian-Hopf bifurcations of four-dimensional symplectic maps”, *Nonlinearity* **17**, 691–710 (2004).
- ⁵¹R. Bartolini, A. Bazzani, M. Giovannozzi, W. Scandale, and E. Toderico, “Tune evaluation in simulations and experiments”, *Part. Accel.* **52**, 147–177 (1996).
- ⁵²M. Born, *The Mechanics of the Atom*, G. Bell & Sons, Ltd., London (1927).
- ⁵³S. Gekle, J. Main, T. Bartsch, and T. Uzer, “Hydrogen atom in crossed electric and magnetic fields: Phase space topology and torus quantization via periodic orbits”, *Phys. Rev. A* **75**, 023406 (2007).
- ⁵⁴À. Jorba, “Numerical computation of the normal behaviour of invariant curves of n -dimensional maps”, *Nonlinearity* **14**, 943–976 (2001).
- ⁵⁵F. Onken, *Bifurcations of families of 1-tori in 4D symplectic maps*, Masterthesis, Technische Universität Dresden, Fachrichtung Physik (2015).
- ⁵⁶H. Schomerus, “Semiclassical interference of bifurcations”, *Europhys. Lett.* **38**, 423 (1997).
- ⁵⁷A. Bäcker, *Classical and Quantum Chaos in Billiards*, Ph.D. thesis, Abteilung Theoretische Physik, Universität Ulm (1998).
- ⁵⁸A. J. Lichtenberg and M. A. Leiberman, *Regular and Chaotic Dynamics*, Springer-Verlag, New York, second edition (1992).
- ⁵⁹P. A. Patsis and L. Zachilas, “Using color and rotation for visualizing four-dimensional Poincaré cross-sections: With applications to the orbital behavior of a three-dimensional Hamiltonian system”, *Int. J. Bifurcat. Chaos* **4**, 1399–1424 (1994).
- ⁶⁰P. Ramachandran and G. Varoquaux, “Mayavi: 3D visualization of scientific data”, *Comput. Sci. Eng.* **13**, 40–51 (2011).
- ⁶¹R. Rimmer, “Symmetry and bifurcation of fixed points of area preserving maps”, *J. Diff. Eqs.* **29**, 329–344 (1978).
- ⁶²M. A. M. de Aguiar, C. P. Malta, M. Baranger, and K. T. R. Davies, “Bifurcations of periodic trajectories in non-integrable Hamiltonian systems with two degrees of freedom: Numerical and analytical results”, *Ann. Phys. (N.Y.)* **180**, 167–205 (1987).
- ⁶³J. A. G. Roberts and G. R. W. Quispel, “Chaos and time-reversal symmetry. Order and chaos in reversible dynamical systems”, *Phys. Rep.* **216**, 63–177 (1992).
- ⁶⁴J. S. W. Lamb, “Reversing symmetries in dynamical systems”, *J. Phys. A* **25**, 925–937 (1992).
- ⁶⁵E. Piña and L. Jiménez Lara, “On the symmetry lines of the standard mapping”, *Physica D* **26**, 369–378 (1987).
- ⁶⁶E. Castellá and À. Jorba, “On the vertical families of two-dimensional tori near the triangular points of the bicircular problem”, *Celest. Mech. Dyn. Astr.* **76**, 35–54 (2000).